This article has been accepted for publication in a future issue of this journal, but has not been fully edited. Content may change prior to final publication. Citation information: DOI 10.1109/TEC.2021.3138465, IEEE Transactions on Energy Conversion

An Axial-Flux Dual-Rotor Slotless Permanent Magnet Motor with Novel Equidirectional Toroidal Winding

Jikai Si, *Member*, *IEEE*, Tianxiang Zhang, Yihua Hu, *Senior Member*, *IEEE*, Chun Gan, *Member*, *IEEE*, and Yingsheng Li

***Abstract*—In this paper, a dual-rotor slotless axial-flux permanent magnet (AFPM) motor with equidirectional toroidal winding (ED-TW) is proposed and compared with the AFPM motor with traditional toroidal winding (T-TW) with the same dimensions, number of coils and poles. Different from the T-TW, only the positive sides of coils of the ED-TW are left on one side of the stator core, the return sides of the coils are all removed to the other side of the stator core. Firstly, the structure and operation principle of the two motors are introduced and analyzed. To clarify the features of the ED-TW, the synthetic electromotive force (EMF) vector and armature reaction field of the ED-TW and T-TW are studied. Secondly, the main size equations of the AFPM motors with toroidal windings are presented. Subsequently, the electromagnetic characteristics of the AFPM motors with ED-TW and T-TW are analyzed and compared based on the three-dimensional finite element method (3D-FEM). The comparison results indicate that the AFPM motor with ED-TW has superiority in torque density and efficiency. Finally, a prototype of the AFPM motor with ED-TW is manufactured and tested, which validates the feasibility of the proposed motor and the correctness of the analysis of the 3D-FEM.**

***Index Terms*—Axial-flux permanent magnet motor, back-EMF, dual rotor, electromagnetic characteristics, equidirectional toroidal winding, torque density.**

I. Introduction

In recent years, electrification of transportation has been intensively investigated to cope with environmental pollution and energy shortage problems [1]-[3]. Road transport accounts for nearly 75 % of the total greenhouse gas (GHG) emissions [4]. Electric vehicle (EV) and hybrid electric vehicle (HEV) offer a promising solution to the challenge of GHG emissions due to its higher efficiency and less dependent on conventional sources of energy [5]. As an energy conversion device, traction motor is one of the most important subsystems of powertrain of EV and HEV. Thanks to the merits of high torque density, high efficiency and power factor, permanent magnet (PM) motors have been widely applied in EV and HEV [6]-[11]. They can be mainly classified into radial flux PM (RFPM) motors and axial flux PM (AFPM) motors, according to the direction of flux in the air gap. It is demonstrated that AFPM motors have distinct advantages compared with RFPM motors, including higher torque density, higher efficiency and more compact structure [12], [13]. Therefore, AFPM motors are getting more attention from researchers.

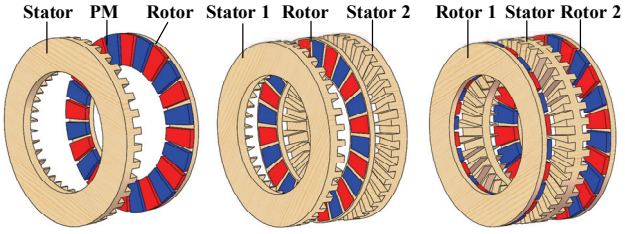

Fig. 1. AFPM motors with (a) single-stator and single-rotor, (b) dual-stator and single-rotor, (c) single-stator and dual-rotor.

In the past decade, many researchers have made important contributions on AFPM motors [14]-[22]. In [17], an AFPM motor with single-stator and single-rotor is proposed. It has the merits of compact structure and low cogging torque, but it inevitably has the disadvantages of low torque density and high axial magnetic pull due to its single-stator single-rotor structure [18]. To solve these problems, dual-stator single-rotor structure and single-stator dual-rotor structure are increasingly combined with AFPM motors [19]-[22]. Fig. 1 shows the AFPM motors with single-stator single-rotor, dual-stator single-rotor and single-stator dual-rotor. Compared with dual-stator single-rotor structure, the AFPM motor with single-stator and dual-rotor is preferred for EV drive applications due to its better power density and thermal capability [20]. In addition, the winding structure of the motor proposed in [21] is overlap winding, which has the disadvantages of long end winding and high copper loss. The single-stator dual-rotor AFPM motor with non-overlap concentrated winding including tooth-wound or toroidal windings are gaining popularity due to their relatively short end winding and low copper loss. In [22], a single-stator dual-rotor AFPM motor with toroidal winding (core-wound) is analyzed. It is shown that, compared with tooth-wound winding, toroidal winding requires 16 % less copper for the end winding

Manuscript received July 13, 2021; revised November 23, 2021; accepted December 19, 2021. This work is partially supported by Natural Science Foundation of China under grant No.51777060, in part by the Major Special Project for Collaborative Innovation in Zhengzhou No. 20XTZX12023. (Corresponding author: Tianxiang Zhang)

Jikai Si and Tianxiang Zhang are with the Zhengzhou University, Zhengzhou, 450001, China (e-mail: sijikai@zzu.edu.cn; zhangtianxiang@gs.zzu.edu.cn).

Yihua Hu is with the University of York, York, YO105DD, UK (e-mail: yihua.hu@york.ac.uk).

Chun Gan is with the Huazhong University of Science and Technology, Wuhan, 430074, China (e-mail: chungan@hust.edu.cn).

Yingsheng Li is with the Zhengzhou Runhua Intelligent Equipment Co., Ltd. Zhengzhou, 450004, China (e-mail: xdlys@vip.sina.com).

This article has been accepted for publication in a future issue of this journal, but has not been fully edited. Content may change prior to final publication. Citation information: DOI 10.1109/TEC.2021.3138465, IEEE Transactions on Energy Conversion

in certain slot/pole/phase combination, which could indirectly improve the torque density. Fig. 2 shows the single-stator dual-rotor AFPM motors with overlap, tooth wound and toroidal windings. The characteristics of different winding structures are summarized in TABLE I. It should be noted that the end-winding length and cooper loss of toroidal winding are not always shorter and lower than these of the tooth-wound winding, it determined by the slot/pole/phase combination and the parameters of stator, which is illustrated in [22].

TABLE I
CHARACTERISTICS OF DIFFERENT WINDING STRUCTURE

Winding structure	Length of end winding	Copper loss
Overlap winding	long	high
Tooth-wound winding	mid	mid
Toroidal winding (core-wound)	short	low

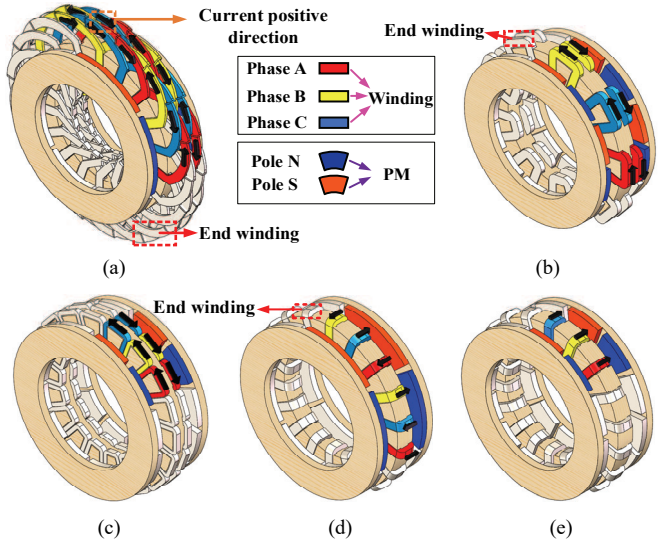

Fig. 2. Single-stator dual-rotor AFPM motors with (a) overlap winding. (b) single-layer tooth-wound winding. (c) double-layer tooth-wound winding. (d) toroidal winding (core-wound). (e) ED-TW (core-wound).

To further improve torque density, an equidirectional toroidal-winding (ED-TW) structure is proposed in [23]-[26] by our research team, which are used for RFPM motor and generator, respectively. The meaning of ED-TW is as follows:

1) The winding direction of all coils is identical.
2) All the coils of each phase have the same positive current direction.
3) All the coils in a phase have the identical current direction at the same time.

It is shown that the RFPM motor with ED-TW has a significant improvement in torque density than the RFPM motor with traditional toroidal or tooth-wound windings. However, the motor which proposed in [23] has the disadvantages of high torque ripple and low winding utilization rate due to its slotted and single-rotor structure. Compared with slotted motor, slotless motor has the merits of zero-cogging for a smooth operation [27]. In addition, dual-rotor structure could make full use of both sides of the ED-TW. Hence, the ED-TW structure is greatly suitable for single-stator dual-rotor slotless AFPM motor, which could take full advantage of the ED-TW. The single-stator dual-rotor AFPM motor with ED-TW is shown in Fig. 2(e). Unlike the other windings shown in Fig. 2, only the positive sides of the ED-TW are left on one side of the stator core and the return sides of the ED-TW are all removed to the other side of the stator core. If the ED-TW structure is combined with a single-stator dual-rotor slotless AFPM motor, it is going to be a new way to increase the torque density of such a AFPM motor. Additionally, owing to the special winding layout of the ED-TW, the synthetic electromotive force (EMF), armature reaction field and size equations of the motor with ED-TW may be changed. Therefore, a dual-rotor slotless axial-flux permanent magnet (AFPM) motor with equidirectional toroidal winding (ED-TW) is proposed and compared with the dual-rotor slotless AFPM motor with traditional toroidal winding (T-TW) which has both positive and return sides of the coils on one side of the stator core. The two motors have the same dimensions, number of coils and poles.

This paper is organized as follows: The structure and operation principle of the AFPM motors with ED-TW and T-TW are clarified in Section II. In Section III, the main size equations of the proposed motor are presented. The differences and similarities between AFPM motors with ED-TW and T-TW in structure, size equations, etc., are summarized in Section IV. In Section V, the electromagnetic characteristics of the AFPM motors with ED-TW and T-TW are analyzed and compared based on three-dimensional finite element method (3D-FEM). The experimental test of the AFPM motor with ED-TW is implemented in Section VI. Finally, Section VII exhibits some conclusions.

II. STRUCTURE AND OPERATION PRINCIPLE OF THE PROPOSED MOTOR

A. Motor Structure

The topologies of the AFPM motors with ED-TW and T-TW are shown in Fig. 3. It can be seen that the structures of the two motors are similar, including two rotors and one stator which is sandwiched in the middle. The surface mounted PMs are distributed on the rotors along the circumference, and adjacent PMs are of opposite polarity. The stator is constructed with no slot, and the toroidal windings are pasted directly on the stator core with epoxy, which has the advantages of no cogging torque and short end winding.

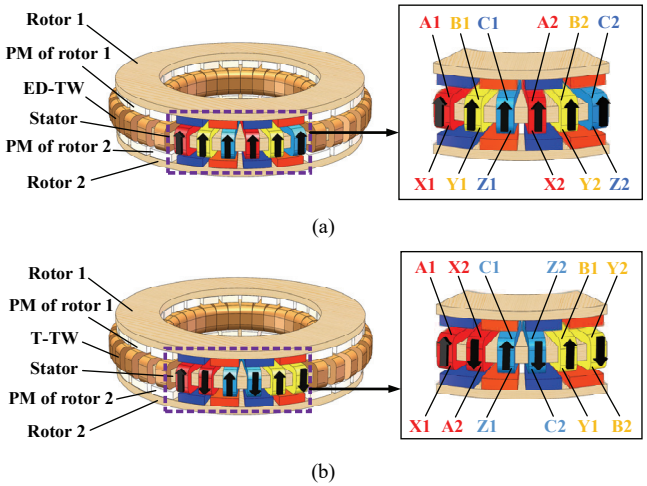

Fig. 3. Topologies of the AFPM motors with (a) ED-TW. (b) T-TW.

B. Winding Layout

As shown in Fig. 4, the winding layout of 1/6 models (six coils, two pole pairs) of the ED-TW and the T-TW are depicted.

This article has been accepted for publication in a future issue of this journal, but has not been fully edited. Content may change prior to final publication. Citation information: DOI 10.1109/TEC.2021.3138465, IEEE Transactions on Energy Conversion

Different from the T-TW, the positive sides of the coils (A, B, and C) of the ED-TW are all on the same side of the stator core. Accordingly, the return sides of the coils (X, Y, and Z) of the ED-TW are all on the other side of the stator core.

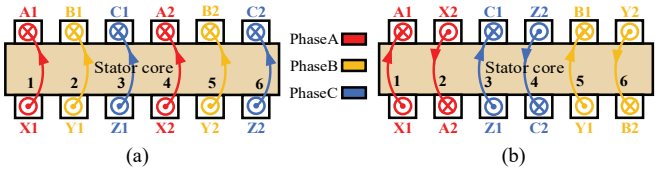

Fig. 4. Winding layout of the two winding types. (a) ED-TW. (b) T-TW.

To further illustrate the structure characteristics of the ED-TW, the three-phase synthetic EMF vector diagram and winding connection schematic of the 1/6 model of the AFPM motor with ED-TW are shown in Fig. 5. The degrees shown in Fig. 5 are electrical degrees. It can be seen that the synthetic EMF of positive sides of coil (E_A, E_B, and E_C) are all on one side of the stator core, and the synthetic-EMF of return sides of coil (E_X, E_Y, and E_Z) are all on the other side of the stator core due to the special layout of the ED-TW. The advantage of this layout is that there is no phase difference between each coil-EMF in one phase due to its three-coils and two-poles combination (minimum unit motor), which can be considered that the distribution factor could be ignored. In addition, for the toroidal windings, the two (negative and return) sides of each coil are on the different side of the stator core that the coil-EMF of two sides of one coil has no contribution to each other. Therefore, the pitch factor of the AFPM motor with toroidal winding should be 0.5. In addition, the winding connection can be observed that the incoming line terminals (A1, B1, and C1) are connected to a three-phase power source, and the out coming line terminals (X2, Y2, and Z2) are connected in wye connection.

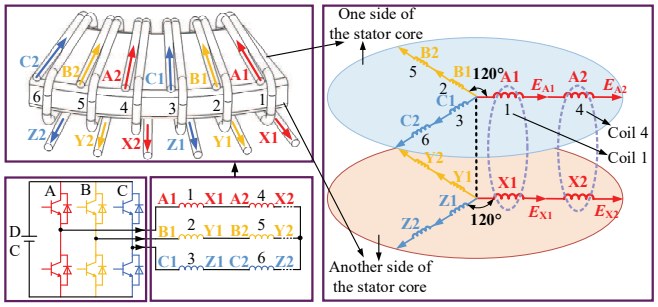

Fig. 5. Three-phase synthetic-EMF vector diagram and winding connection schematic of the 1/6 model of the AFPM motor with ED-TW.

To clarify the advantage of the ED-TW, the A-phase synthetic EMF of the 1/6 models of the AFPM motors with ED-TW and T-TW are compared in Fig. 6. The premise is that the two motors have the same frequency, turns per phase, turns per coil and magnetic flux per pole. In addition, the degrees shown in Fig. 6 are electrical degrees. It is shown that there is no phase difference between the two coil-EMF (both of them are induced by the positive side of coils) in phase A of the AFPM motor with ED-TW. However, there is 120 electrical degrees phase difference between the two coil-EMF (one of them induced by the positive side of coil 1, the other is induced by the return side of coil 2) in phase A of the AFPM motor with T-TW. The coefficient to represent the reduction in the synthetic EMF due to the phase difference between the two coils could be called distribution factor. For the AFPM motor with ED-TW, there is no phase difference between each coil-EMF in one phase due to the special coil layout of the ED-TW and the three-coil two-pole combination of the minimum unit motor, the effect of distribution factor on the synthetic EMF could be ignored. Therefore, the AFPM motor with ED-TW could obtain a larger phase synthetic EMF than the AFPM motor with T-TW.

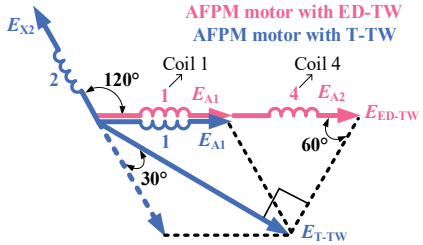

Fig. 6. A-phase synthetic EMF vector diagram of the 1/6 model of the two motors on one side of the stator core.

The root-mean-square (RMS) of no-load phase back-EMF of one side of a coil of the slotless AFPM motor with toroidal winding can be expressed as [28]

$$E_c = \frac{2}{\pi}\Omega B_g \int_{R_i}^{R_o} \frac{\sin(\frac{w_c \cdot p}{2r})}{\sin(\frac{w_c \cdot p}{2rN_c})} r dr \quad (1)$$

where, Ω is the mechanical angular velocity of the motor, B_g is the fundamental harmonic amplitude of the air gap flux density, R_o is the outer radius of the stator core, R_i is the inner radius of the stator core, N_c is the number of turns per coil, w_c is the width of the coil, p is the number of pole pairs, r is the radius of the coil at different positions along the radial direction.

According to Fig. 6, the RMS of no-load phase back-EMF of the 1/6 model of the AFPM motor with ED-TW can be expressed as

$$E_{\text{ED-TW}} = E_c + E_c = \frac{4}{\pi}\Omega B_g \int_{R_i}^{R_o} \frac{\sin(\frac{w_c \cdot p}{2r})}{\sin(\frac{w_c \cdot p}{2rN_c})} r dr \quad (2)$$

The RMS of no-load phase back-EMF of the 1/6 model of the AFPM motor with T-TW is

$$E_{\text{T-TW}} = (E_c + E_c)\underbrace{\sin\frac{\pi}{3}}_{K_d} = \frac{2\sqrt{3}}{\pi}\Omega B_g \int_{R_i}^{R_o} \frac{\sin(\frac{w_c \cdot p}{2r})}{\sin(\frac{w_c \cdot p}{2rN_c})} r dr \quad (3)$$

where, K_d is the distribution factor.

If the Ω, N_c, R_o, R_i, B_g, p, and w_c of both motors are the same, it can be concluded that the RMS of no-load phase back-EMF of the AFPM motor with ED-TW is 15.47 % higher than that of the AFPM motor with T-TW since there is no phase difference between each coil-EMF in phase A of the ED-TW.

C. Operation Principle

To illustrate the operation principle of the AFPM motors with ED-TW and T-TW clearly, the 1/6 models of both motors are taken as an example to analyze the armature reaction field at different times in a period. The minimum unit structure of the AFPM motor with ED-TW consists of three coils and one pole pair, hence, the 1/6 model of the AFPM motor with ED-TW

This article has been accepted for publication in a future issue of this journal, but has not been fully edited. Content may change prior to final publication. Citation information: DOI 10.1109/TEC.2021.3138465, IEEE Transactions on Energy Conversion

contains two minimum unit structures. However, the minimum unit motor of the AFPM motor with T-TW consists of six coils and two pole pairs, which equal the number of coils and pole pairs of the 1/6 model. Fig. 7 shows the three-phase sinusoidal alternating current waveforms. As shown in Fig. 7, a period is divided into three different times, and the three-phase current directions at the corresponding times are shown in TABLE II.

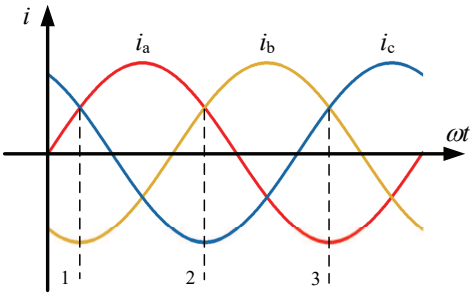

Fig. 7. Three-phase sinusoidal alternating current waveforms.

TABLE II
CURRENT DIRECTION OF THREE-PHASE WINDINGS AT DIFFERENT TIMES

Current	Time		
	1	2	3
i_a	+	+	−
i_b	−	+	+
i_c	+	−	+

The armature reaction field produced by phase A of the ED-TW and T-TW at time 1 are shown in Fig. 8. The current direction '+' is defined as the current inflow plane, and the current direction '−' is defined as the current outflow plane. As shown in Fig. 8, for the T-TW, the flux path of the A-phase armature reaction field is similar to that of the two mutually repulsive magnets, and the magnetic poles can be produced on both sides of the stator core. For the ED-TW, due to its special winding layout, the flux path of A-phase armature reaction field is similar to that of the two mutually attract magnets, and there are no magnetic poles on both sides of the stator core. The ED-TW can produce magnetic poles continuously on both sides of the stator core only under the combined action of phase A, B and C armature reaction fields. Therefore, the principles of the armature reaction field produced by the ED-TW and T-TW are different.

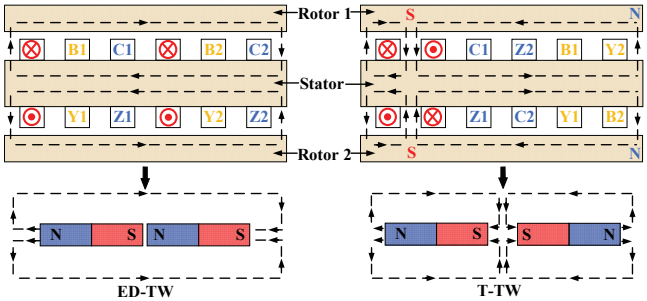

Fig. 8. Armature reaction fields produced by phase A of the ED-TW and T-TW at time 1.

According to the current direction shown in TABLE II, the armature reaction field produced by phase A, B, and C of the ED-TW and T-TW at time 1 to time 3 can be obtained, which is shown in Fig. 9. To facilitate the display of the armature reaction field produced by the ED-TW and T-TW on both sides of the stator, the schematic is the radial unfold diagram of the stator. It is shown that, from time 1 to time 3, the pole N and pole S are gradually moved to the right, i.e., the armature reaction fields are rotated counterclockwise. Therefore, the armature reaction fields produced by the ED-TW and T-TW rotate periodically with time. Meanwhile, it can be seen that the armature reaction fields of both sides of the stator core have the same polarity, and rotate in the same direction.

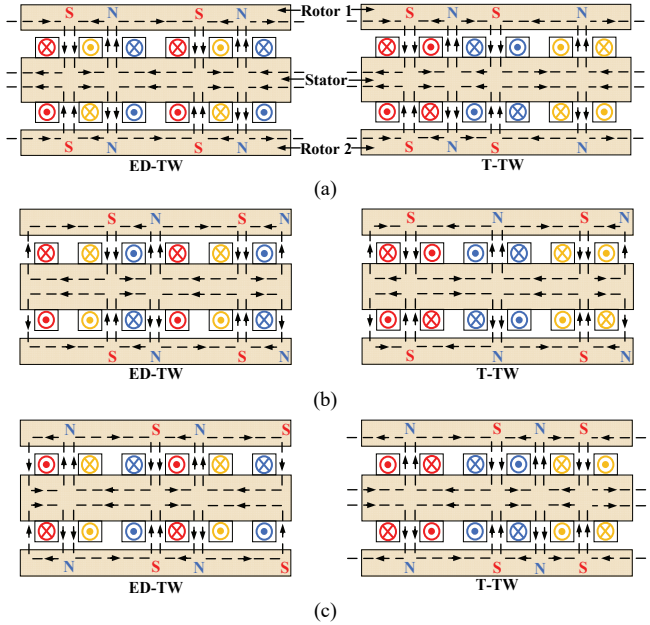

Fig. 9. Armature reaction field produced by phase A, B and C of the ED-TW and T-TW at different times. (a) time 1. (b) time 2. (c) time 3.

The flux distribution produced by PMs of the two motors is the same, which is shown in Fig. 10. It is shown that the PMs of both rotors are distributed symmetrically along the axial direction. The PMs in the same axial direction have the identical magnetic poles, which is the N-N poles type. In addition, both sides of the stator core of each motor will produce two rotating armature reaction fields with the same rotating speed and direction when the three-phase current is fed into the ED-TW and T-TW, respectively, which is shown in Fig. 9. Consequently, the two rotors will rotate synchronously with the interaction between the armature reaction field and PMs field.

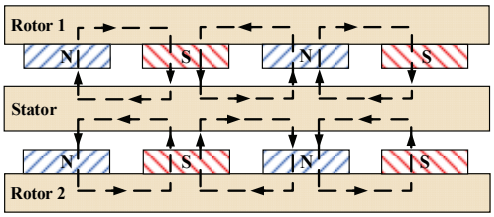

Fig. 10. Flux distribution produced by PMs of the two motors.

III. DESIGN OF THE PROPOSED MOTOR

The rotor on both sides of the dual-rotor AFPM motor is symmetrical, hence, it can be designed according to the structure of single-stator and single-rotor.

If the stator leakage inductance and resistance are neglected, the output power P_{out} of the AFPM motors can be expressed as [29]

$$P_{out} = \eta \frac{m}{T} \int_0^T e(t) i(t) \mathrm{d}t = \eta m K_p E_{pk} I_{pk} \tag{4}$$

This article has been accepted for publication in a future issue of this journal, but has not been fully edited. Content may change prior to final publication. Citation information: DOI 10.1109/TEC.2021.3138465, IEEE Transactions on Energy Conversion

where, η is the motor efficiency, m is the number of phases of the motor, T is the period of one cycle of the EMF, $e(t)$ is the phase EMF, $i(t)$ is the phase current, I_{pk} is the peak value of the phase current, E_{pk} is the peak value of the phase EMF, K_p is the electrical power waveform factor and it can be expressed as

$$K_p = \frac{1}{T}\int_0^T \frac{e(t)i(t)}{E_{pk}I_{pk}}\mathrm{d}t \tag{5}$$

The peak value of the phase EMF E_{pk} of the AFPM motor can be defined as

$$E_{pk} = \frac{\pi}{2}K_w N_{ph} B_g \frac{f}{p}(1-K_r^2)D_o^2 \tag{6}$$

where, K_w is the winding factor, N_{ph} is the number of turns per phase, f is the frequency of the motor, K_r is the ratio of inner diameter to outer diameter of the stator core, D_o is the outer diameter of the stator core.

A. Size equations of the AFPM motors which are suitable for the tooth-wound or overlap windings

For the AFPM motors, the electrical loading A is a function of radius and can be expressed as [30]

$$A = 2mN_{ph}\frac{I_{rms}}{\pi D_{avg}} \tag{7}$$

where, I_{rms} is the RMS of the phase current, D_{avg} is the average value of the inner and outer diameters of the stator core.

The phase current peak value can be obtained from Equation (7), and as shown below

$$I_{pk} = \frac{\sqrt{2}\pi A D_{avg}}{2mN_{ph}} = \frac{\sqrt{2}\pi A(1+K_r)D_o}{4mN_{ph}} \tag{8}$$

Combine Equations (4)-(8), the output power P_{out} and torque T_{out} of the AFPM motors can be expressed as

$$P_{out} = \frac{\sqrt{2}}{8}\pi^2\eta K_p K_w B_g A \frac{f}{p}\left(1-K_r^2\right)\left(1+K_r\right)D_o^3 \tag{9}$$

$$T_{out} = \frac{\sqrt{2}}{16}\pi\eta K_p K_w B_g A\left(1-K_r^2\right)\left(1+K_r\right)D_o^3 \tag{10}$$

B. Adjusted size equations of the AFPM motors with toroidal winding

It should be noted that the Equation (7)-(10) are not suitable for the AFPM motors with toroidal winding including ED-TW and T-TW. Therefore, it is necessary to illustrate the adjusted size equations of the AFPM motors with toroidal winding in this paper.

The critical point lies in the fact that the relationship between the number of turns per phase N_{ph} and the number of total effective conductors on one side of the stator core. The Equation (7) is suitable for the AFPM motor with windings that two sides of one coil are all on the one side of the stator core like tooth-wound winding or overlap winding. As shown in Equation (7), the $2mN_{ph}$ means that the total number of effective conductors on one side of the stator core, which could consider the two-side conductors of one coil on one side of the stator core.

Fig. 11 shows the stator structure schematic of the AFPM motors with ED-TW and T-TW. As shown in Fig. 11, the number of turns per coil of the two windings are both 2 and the number of coils per phase are 2 either. Therefore, the N_{ph} of the ED-TW and T-TW are both 4. For the AFPM motors with toroidal winding, the total number of effective conductors on one side of the stator core equals the product of the number of phase m and the N_{ph}. Hence, the electric loading A_{TW} of the AFPM motors with toroidal winding should be adjusted as

$$A_{TW} = mN_{ph}\frac{I_{rms}}{\pi D_{avg}} \tag{11}$$

The phase current peak value $I_{pk\text{-}TW}$ of the AFPM motors with toroidal winding can be expressed as

$$I_{pk\text{-}TW} = \frac{\sqrt{2}\pi A D_{avg}}{mN_{ph}} = \frac{\sqrt{2}\pi A(1+K_r)D_o}{2mN_{ph}} \tag{12}$$

Combine Equations (4)-(6), (11), (12), the output power $P_{out\text{-}TW}$ and torque $T_{out\text{-}TW}$ of the AFPM motors with toroidal winding can be defined as

$$P_{out\text{-}TW} = \frac{\sqrt{2}}{4}\pi^2\eta K_p K_w B_g A \frac{f}{p}\left(1-K_r^2\right)\left(1+K_r\right)D_o^3 \tag{13}$$

$$T_{out\text{-}TW} = \frac{\sqrt{2}}{8}\pi\eta K_p K_w B_g A\left(1-K_r^2\right)\left(1+K_r\right)D_o^3 \tag{14}$$

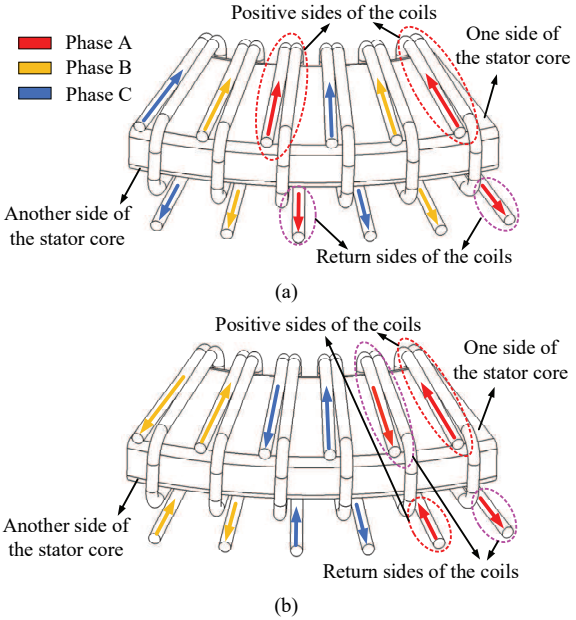

Fig. 11. Stator structure schematic of the AFPM motors with (a) ED-TW. (b) T-TW.

C. Primary parameters of the AFPM motors

To verify the reasonability of the proposed motor, the characteristics of the AFPM motor with ED-TW are compared with that of the AFPM motor with T-TW. The design of the two motors needs to follow some preconditions to ensure a fair comparison.

1) The two motors have the same dimensions, including outer diameter and inner diameter of the stator and rotors, axial length, PM height and so on.
2) The two motors are excited by the same current source and have the same electric loading.

Based on the principles above, the primary parameters of the AFPM motors with ED-TW and T-TW are presented in TABLE III.

This article has been accepted for publication in a future issue of this journal, but has not been fully edited. Content may change prior to final publication. Citation information: DOI 10.1109/TEC.2021.3138465, IEEE Transactions on Energy Conversion

TABLE III
PRIMARY PARAMETERS OF THE TWO MOTORS

Parameters	AFPM motor with ED-TW	AFPM motor with T-TW
Rated speed	400 rpm	400 rpm
Rated frequency	80 Hz	80 Hz
Rated current (RMS)	10 A	10 A
No. of pole pairs (p)	12	12
No. of winding coils	36	36
Turns of per coil (N_c)	51	51
Turns per phase (N_{ph})	612	612
Electric loading (A)	29.52 kA/m	29.52 kA/m
Outer diameter of stator core (D_o)	240 mm	240 mm
Inner diameter of stator core	156 mm	156 mm
Air-gap length	1 mm	1 mm
Winding thickness	7 mm	7 mm
Winding width (w_c)	12 mm	12 mm
PM height	8 mm	8 mm
Axial length	58 mm	58 mm
Material of stator core	50WW310	50WW310
Material of PM	N48SH	N48SH

IV. DISCUSSION OF THE FEATURES OF THE AFPM MOTORS WITH ED-TW AND T-TW

According to the aforementioned analysis in Section II and Section III, it can be seen that there are some differences and similarities between the AFPM motors with ED-TW and T-TW. The main features focus on the winding layout, synthetic EMF, armature reaction field and size equations. The discussion on these four aspects are as follows:

1) The fundamental difference between the AFPM motors is the change of layout of winding. For the T-TW, there are both positive and return sides of the coils on one side of the stator core. Different from the T-TW, for the ED-TW, only positive sides of the coils are left on the one side of the stator core, the return sides of the coils are all removed to the other side of the stator core. This resulted in the difference of other two aspects between the AFPM motors with ED-TW and T-W.
2) Owing to the special layout of the ED-TW, the synthetic EMF induced by positive sides of the coils (E_A, E_B and E_C) are all on the same side of the stator core, and that induced by return sides of the coils (E_X, E_Y and E_Z) are all on the other side of the stator core. This is different from the AFPM motor with T-W. In addition, on one side of the stator core, there is no phase difference between the EMF induced by each coil of one phase of the ED-TW since the coil and pole combination of minimum unit motor is three coils and two poles. Hence, it could be considered that the distribution factor could be ignored and the three-coils and two-poles combination is greatly suitable for the ED-TW. Compared with the AFPM motor with T-TW, the AFPM motor with ED-TW could obtain a larger phase synthetic EMF.
3) When only one phase coils are energized, the ED-TW does not produce magnetic poles on either side of the stator core due to its special winding layout. Therefore, the three-phase ED-TW could produce magnetic poles continuously on both sides of the stator core only under the combined action of phase A, B and C armature reaction fields. This result in the three-phase ED-TW has the feature that one-pole-pair armature reaction fields on each side of the stator core can be produced by just three coils.
4) The size equations of the AFPM motor with ED-TW and T-TW are the same. But the size equations of the two motors are both different from the size equations which are suitable for the AFPM motors with tooth-wound or overlap winding due to the one-side total conductors of the AFPM motor with toroidal winding equal the product of the number of phase m and the number of turns per phase N_{ph}, and do not need to double it.

In addition, due to the special layout of the ED-TW, it will lead to the difference of electromagnetic characteristics between the AFPM motors with ED-TW and T-TW (e.g., no-load back-EMF, torque and so on). Therefore, the electromagnetic characteristics of the two motors should be analyzed and compared, which are presented in Section V.

V. ELECTROMAGNETIC CHARACTERISTICS ANALYSIS

Based on the primary parameters of the two motors presented in TABLE III, the 3D finite element models of the two motors are built. Subsequently, the armature reaction field, no-load and on-load characteristics of the two motors are analyzed by 3D-FEM, respectively.

A. Armature Reaction Field

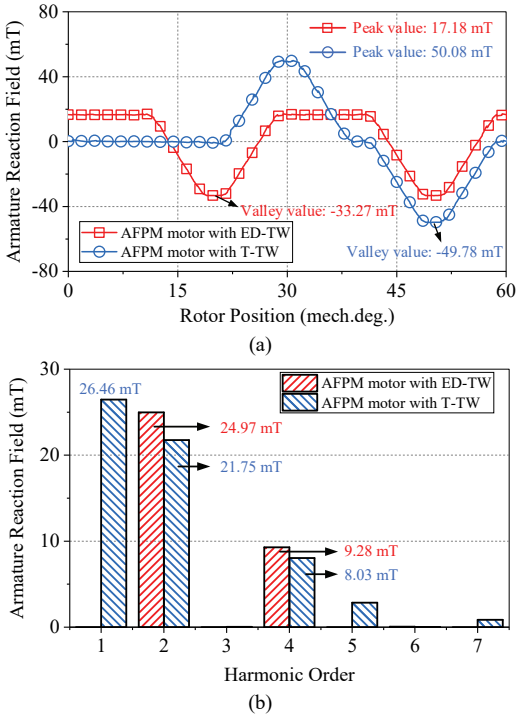

Fig. 12. Armature reaction fields of the AFPM motors with ED-TW and T-TW. (a) Waveforms. (b) Harmonic spectra.

Fig. 12 shows the armature reaction fields at rated current (RMS: 10 A) of the two motors. The armature reaction field characteristics of the two motors are summarized in TABLE IV. For the AFPM motor with ED-TW, the minimum unit motor contains three coils and one pole pair of PMs. The whole AFPM motor with ED-TW proposed in this paper consists of 12 minimum unit motors. Therefore, there are six coils and two pole pairs of PMs in the range of 60 mechanical degrees of the AFPM motor with ED-TW. As shown in Fig. 12(b), the main working armature reaction field harmonic of the AFPM motor with ED-TW is 2nd, which equals the number of pole pairs in

This article has been accepted for publication in a future issue of this journal, but has not been fully edited. Content may change prior to final publication. Citation information: DOI 10.1109/TEC.2021.3138465, IEEE Transactions on Energy Conversion

the range of 60 mechanical degrees. In addition, the amplitude of the 4th harmonic of the AFPM motor with ED-TW is 9.28 mT, which accounted for 37.16 % of the 2nd harmonic. For the AFPM motor with T-TW, the minimum unit motor contains six coils and two pole pairs. The whole AFPM motor with T-TW consists of 6 minimum unit motors. As can be seen, for the AFPM motor with T-TW, the 1st and 2nd harmonics are the main components of the armature reaction field, which are 26.46 and 21.75 mT, respectively. There are two pole pairs of PMs in the range of 60 mechanical degrees. Therefore, the 2nd harmonic is the main working armature reaction field harmonic of the AFPM motor with T-TW. It can be seen from TABLE IV that the main working armature reaction field of the AFPM motor with ED-TW is 14.80 % higher than that of the AFPM motor with T-TW.

TABLE IV
ARMATURE REACTION FIELD CHARACTERISTICS OF THE TWO MOTORS

	AFPM motor with ED-TW	AFPM motor with T-TW
Main working harmonic	2nd	2nd
Main working harmonic amplitude	24.97 mT	21.75 mT
1st harmonic amplitude	0 mT	26.46 mT
4th harmonic amplitude	9.28 mT	8.03 mT

B. No-load Characteristics

The air-gap flux density and its harmonics spectra produced by PMs of the two motors are presented in Fig. 13. The two motors differ only in the winding structure, hence, the air-gap flux density waveform produced by PMs of the AFPM motors with ED-TW and T-TW are similar. As shown in Fig. 13, the amplitudes of fundamental harmonic of the air-gap flux density in the two motors are both 0.77 T. The total harmonic distortion (THD) of the AFPM motors with ED-TW and T-TW are 23.09 % and 23.03 %, respectively.

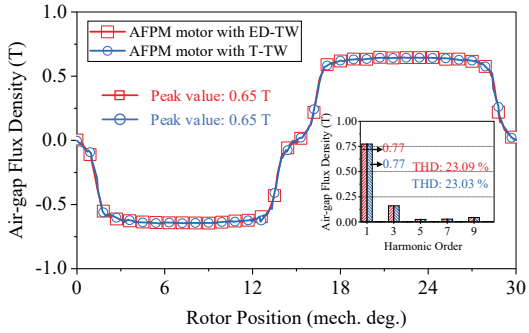

Fig. 13. Air-gap flux density and its harmonics spectra of the two motors.

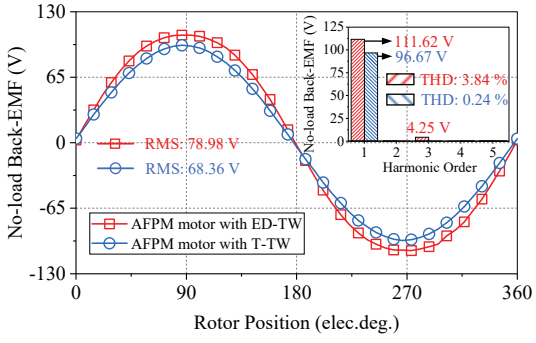

Fig. 14. No-load phase back-EMF and its harmonics spectra of the two motors.

The no-load phase back-EMF and its harmonics spectra of the two motors at rated speed (400 rpm) are presented in Fig. 14. It can be seen that the RMS of the no-load back-EMF of the AFPM motors with ED-TW and T-TW are 78.98 V and 68.36 V, respectively. The amplitudes of the fundamental harmonic of the back-EMF of the AFPM motors with ED-TW and T-TW are 111.62 V and 96.67 V, respectively. Compared with the AFPM motor with T-TW, the RMS of the no-load back-EMF of the AFPM motor with ED-TW is increased by 15.54 %, which validates the correctness of the analysis about the no-load phase back-EMF of the two motors mentioned in Section II. In addition, the THD of the AFPM motors with ED-TW and T-TW are 3.84 % and 0.24 %, respectively. The AFPM motor with ED-TW has 3rd harmonic in the phase back-EMF due to only one coil side of one coil to link the flux of the minimum unit motor, thus the 3rd harmonic cannot be eliminated. But the 3rd harmonic will be eliminated in the line back-EMF, which is shown in Fig. 15.

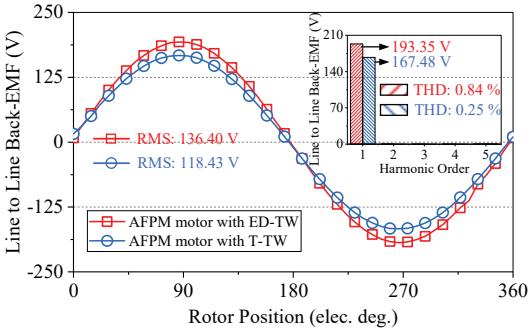

Fig. 15. No-load line back-EMF and its harmonics spectra of the two motors.

According to Equation (2) and Equation (3), the RMS of the no-load phase back-EMF of the AFPM motors with ED-TW and T-TW can be obtained, which is shown in Fig. 16. It is notable that the RMS of the phase back-EMF needs to be calculated by the average value of fundamental harmonic of air-gap flux density in the thickness (axial) range of the winding of the two motors, because the air-gap flux density of the slotless AFPM motor varies nonlinearly in different positions in the axial direction of the winding. The RMS of the no-load phase back-EMF of the AFPM motors with ED-TW and T-TW at rated speed are listed in TABLE V. As can be seen, the no-load phase back-EMF results of calculation of both motors match well with that of the 3D finite element analysis (3D-FEA), and the no-load phase back-EMF of the AFPM motor with ED-TW is always higher than that of the AFPM motor with T-TW in the whole speed range, which further validate the correctness of the analysis mentioned above.

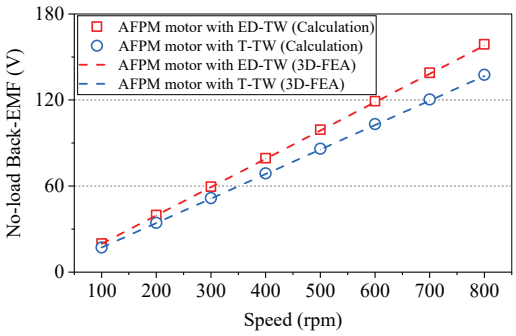

Fig. 16. No-load phase back-EMF variation against speed of the AFPM motors with ED-TW and T-TW.

This article has been accepted for publication in a future issue of this journal, but has not been fully edited. Content may change prior to final publication. Citation information: DOI 10.1109/TEC.2021.3138465, IEEE Transactions on Energy Conversion

TABLE V
NO-LOAD BACK-EMF OF THE TWO MOTORS AT RATED SPEED

No-load back-EMF	AFPM motor with ED-TW	AFPM motor with T-TW
Calculation (RMS)	79.44 V	68.80 V
3D-FEA (RMS)	78.98 V	68.36 V
Relative error	0.58 %	0.64 %

C. On-load Torque Characteristics

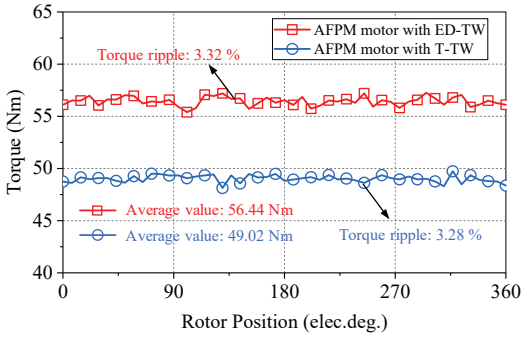

Fig. 17. Torque waveforms of the two motors under rated load condition.

TABLE VI
TORQUE PERFORMANCES OF THE TWO MOTORS

	AFPM motor with ED-TW	AFPM motor with T-TW
Average torque	56.44 Nm	49.02 Nm
Torque constant	5.64 Nm/A	4.90 Nm/A
Average torque density	37.25 kNm/m³	32.35 kNm/m³
Torque ripple	3.32 %	3.28 %

Fig. 17 shows the torque waveforms of the two motors under rated load condition (80 Hz, RMS: 10 A). Additionally, the torque performances of the two motors under rated load condition are listed in TABLE VI. In conclusion, compared with the AFPM motor with T-TW, the average torque density of the AFPM motor with ED-TW is increased by 15.15 % without the aggravation of the torque ripple. Fig. 18 shows the torque-current characteristic of the two motors. It is shown that, within the whole current range, the output torque of the AFPM motor with ED-TW is average 14.51 % higher than that of the AFPM motor with T-TW.

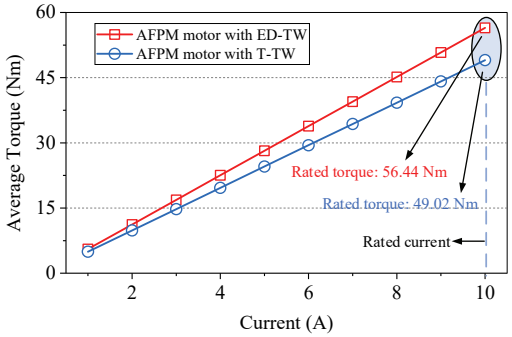

Fig. 18. Torque-current characteristic of the two motors.

D. Loss and Efficiency

Fig. 19 shows the losses of the AFPM motors with ED-TW and T-TW at rated working point (10 Arms, 400 rpm). For the low-speed and high-torque applications, the cooper loss of the AFPM motors accounted for a major proportion of the total loss. It is shown that the two motors have the same cooper loss (419.15 W) due to the length of the effective and end windings of the two motors are the same. The PM loss of the AFPM motor with T-TW is higher than that of the AFPM motor with ED-TW due to the larger armature field subharmonic of the AFPM motor with T-TW. The core loss, PM loss and copper loss are considered in the calculation of efficiency, as

$$\eta = \frac{P_{\text{out}}}{P_{\text{out}} + P_{\text{core}} + P_{\text{PM}} + P_{\text{copper}}} \tag{15}$$

where, P_{core} is the core loss, P_{PM} is the PM loss and P_{copper} is the cooper loss. The output power and efficiency of the two motors at rated working point are summarized in TABLE VII. Thanks to the improvement of the torque and output power, the efficiency of the AFPM motor with ED-TW is 2.08 % high than that of the AFPM motor with T-TW.

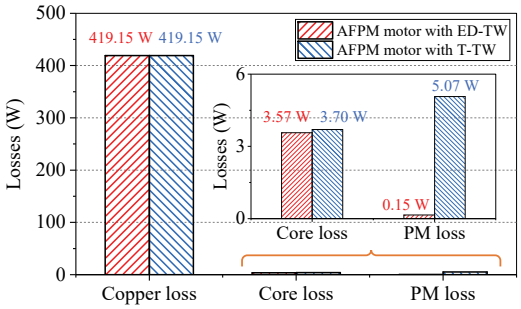

Fig. 19. Losses of the two motors.

TABLE VII
OUTPUT POWER AND EFFICIENCY AT RATED WORKING POINT

	AFPM motor with ED-TW	AFPM motor with T-TW
Output power Pout (W)	2363.98	2053.19
Efficiency (%)	84.83	82.75

VI. EXPERIMENTAL VERIFICATION

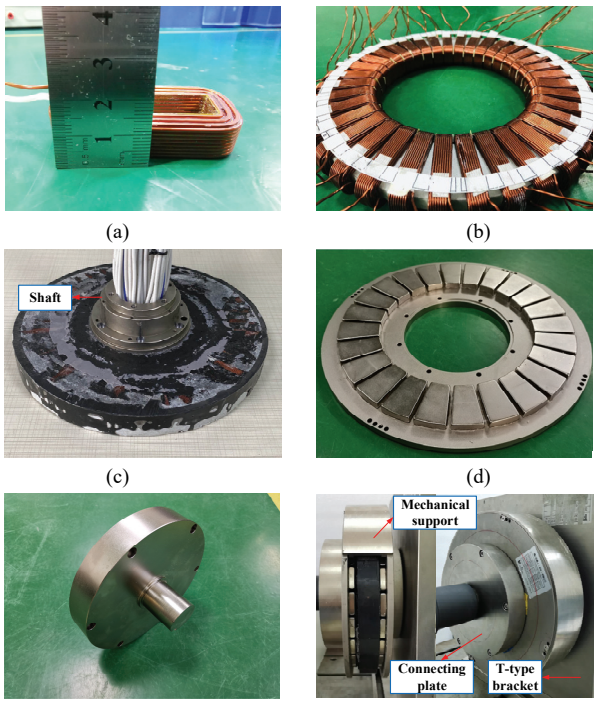

Fig. 20. Prototype of the AFPM motor with ED-TW. (a) Toroidal winding. (b) Stator. (c) Stator encapsulation. (d) Rotor. (e) Connecting plate. (f) Motor assembly.

To validate the foregoing analysis, a prototype of the AFPM motor with ED-TW is manufactured and tested. Fig. 20 shows

This article has been accepted for publication in a future issue of this journal, but has not been fully edited. Content may change prior to final publication. Citation information: DOI 10.1109/TEC.2021.3138465, IEEE Transactions on Energy Conversion

the prototype of the AFPM motor with ED-TW. The winding width is 12 mm, which is shown in Fig. 20(a). As shown in Fig. 20(b), the toroidal windings are pasted directly on the stator core with epoxy. The stator and shaft are encapsulated together by epoxy, which is shown in Fig. 20(c). The stator and shaft are both stationary, and one side of the shaft is fixed to the T-type bracket, which could ensure that the shaft and stator are fixed. The two rotors are connected to the shaft by two bearings and are connected to each other by mechanical support. One rotor is connected to the load by a connecting plate which is fixed on the disc of the rotor and is shown in Fig. 20(f). In addition, the stator core is made of tape wound laminated silicon steel (50WW310). The materials of the rotor core and PM are steel-1010 and N48SH, respectively.

The experimental test platform of the AFPM motor with ED-TW is shown in Fig. 21. It consists of the prototype of the proposed motor, torque transducer (4503A200L00B1000 Kistler), oscilloscope (DL850E Yokogawa) and so on. The drive system of the AFPM motor with ED-TW is presented in Fig. 22. In Fig. 22, i_A, i_B, and i_C are the three-phase currents, i_d, i_q are the dq-axis currents, θ is the rotor position. The SERVOTRONIX CDHD is used to drive the proposed motor. The ATOM-2D2050D1 position encoder is used to measure the rotor position.

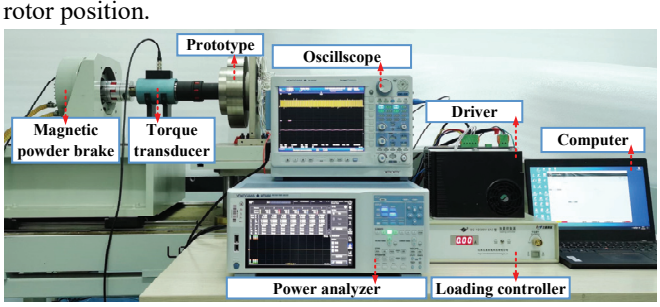

Fig. 21. The experimental test platform of the prototype.

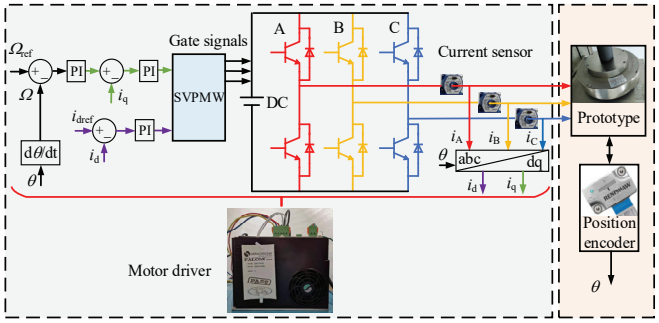

Fig. 22. The drive system of the prototype.

The no-load line to line back-EMF waveforms of the AFPM motor with ED-TW at different speeds are measured, which is shown in Fig. 23. It can be seen that RMS of the no-load line back-EMF of the 3D-FEA and experimental test are 136.41 V and 131.10 V, respectively. The fundamental line back-EMF of the experimental test (193.10 V) agrees well with that of the 3D-FEA (185.40 V), with an error of 3.99 %, which validates the feasibility of the proposed motor and the correctness of the analysis mentioned above. In addition, the THD of the line back-EMF of the 3D-FEA and the test results are 0.61 % and 0.98 %, respectively. As shown in Fig. 23(b), the measured no-load line to line back-EMF matches well with the simulated results.

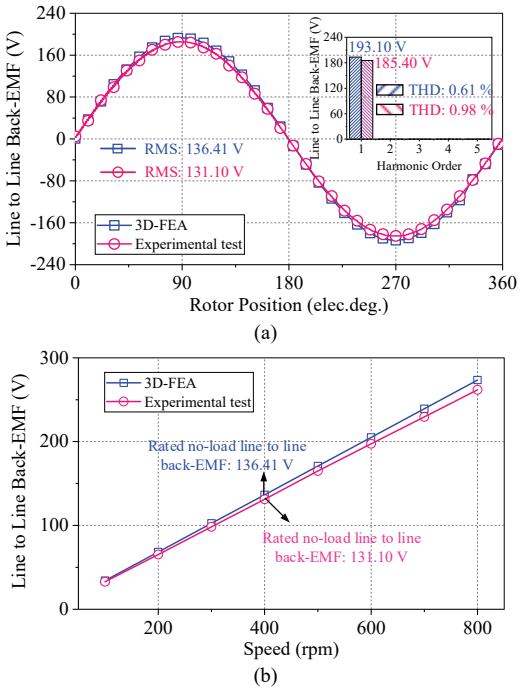

Fig. 23. No-load line to line back-EMF of the AFPM motor with ED-TW. (a) Waveforms under rated speed. (b) RMS variation against speed.

Fig. 24 shows the measured three-phase current of the AFPM motor with ED-TW at rated state. The output torque under rated load condition and the torque-current characteristic of the AFPM motor with ED-TW are shown in Fig. 25(a) and Fig. 25(b), respectively. It is shown that the average value of rated torque of the experimental test is 53.74 Nm, which accounts for 95.22 % that of the 3D-FEA (56.44 Nm). The slight difference between 3D-FEA and experimental test may be the manufacture error and mechanical friction. In addition, the results of torque ripple of the 3D-FEA and experimental test are 3.32 % and 3.62 %, respectively. As shown in Fig. 25(b), the trends of torque versus current of the experimental test and the 3D-FEA are basically consistent. In conclusion, the results of the experimental test agree well with that of the 3D-FEA under no-load and on-load conditions, which validate the feasibility of the proposed motor and the correctness of the 3D-FEA.

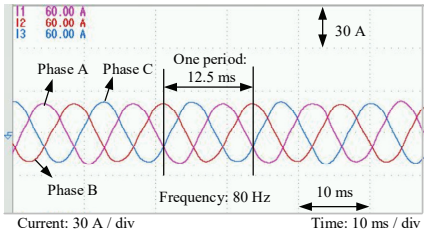

Fig. 24. The measured three-phase current of the prototype at rated state.

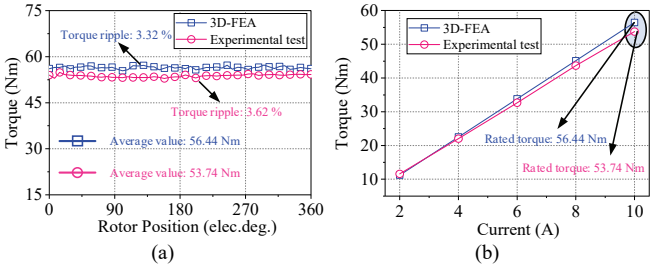

Fig. 25. Output torque of the AFPM motor with ED-TW. (a) Waveforms under rated load condition. (b) Torque-current characteristic.

VII. Conclusion and Discussion

In this paper, a dual-rotor slotless AFPM motor equipped with ED-TW is proposed and compared with the AFPM motor with T-TW. To clarify the features of the ED-TW, the structure, synthetic EMF vector diagram and armature reaction field of the AFPM motors with ED-TW and T-TW are studied. The size equations considering the features of the toroidal winding are presented. Furthermore, the no-load and on-load characteristics of the two motors are analyzed and compared based on 3D-FEM. Finally, the prototype of the AFPM motor with ED-TW is manufactured and tested, which validates the feasibility of the proposed motor and the correctness of the 3D-FEA. Some findings and discussions are summarized as follows:

1) The AFPM motor with ED-TW and T-TW are different in synthetic EMF and the armature reaction field due to the special winding layout of the ED-TW. It can be concluded that the distribution factor of the ED-TW could be ignored and the three-phase and two-poles combination of the minimum unit motor is greatly suitable for the ED-TW. In addition, the AFPM motor with ED-TW and T-TW have similarity in size equations that the one-side electric loading A equal the product of m and N_{ph}, and do not need to double it. It may provide a reference for the researchers in this field to design the motor with the ED-TW.
2) Compared with the AFPM motor with T-TW, the AFPM motor with ED-TW has superiority in back-EMF amplitude, torque density and efficiency because there is no phase difference between the EMF induced by each coil of one phase of the ED-TW. Such the AFPM motor with ED-TW is suitable for low-speed and high-torque applications (e.g., EV, HEV, etc.).
3) This paper focuses on the slotless AFPM motor equipped with ED-TW. To further improve the torque density, the ED-TW could be combined with the slotted AFPM motor, which will be investigated in the following study. This paper lays an important foundation for that.

References

[1] S. I. Kim, S. H. Park, T. S. Park, *et al.*, "Investigation and experimental verification of a novel spoke-type ferrite-magnet motor for electric-vehicle traction drive applications," *IEEE Trans. Ind. Electron.*, vol. 61, DOI 10.1109/TIE.2014.2304697, no. 10, pp. 5763-5770, Oct. 2014.

[2] J. H. Kim, Y. J. Li, and B. Sarlioglu, "Novel six-slot four-pole axial flux-switching permanent magnet machine for electric vehicle," *IEEE Trans. Transport. Electrific.*, vol. 3, DOI 10.1109/TTE.2016.2620169, no. 1, pp. 108-117, Mar, 2017.

[3] R. D. Castro, R. E. Araújo, and D. Freitas, "Wheel slip control of EVs based on sliding mode technique with conditional integrators," *IEEE Trans. Ind. Electron.*, vol. 60, DOI 10.1109/TIE.2012.2202357, no. 8, pp. 3256–3271, Aug. 2013.

[4] J. -R. Riba, C. LApez-Torres, L. Romeral, and A. Garcia, "Rare-earth-free propulsion motors for electric vehicles: A technology review," *Renew. Sustain. Energy Rev.*, vol. 57, DOI 10.1016/j.rser.2015.12.121, pp. 367-379, 2016.

[5] A. Dalal, and P. Kumar, "Design, prototyping, and testing of a dual-rotor motor for electric vehicle application," *IEEE Trans. Ind. Electron.*, vol. 65, DOI 10.1109/TIE.2018.2795586, no. 9, pp. 7185-7192, Sep. 2018.

[6] C. Gong, Y. H. Hu, W. Z. Li, *et al*., "Hybrid DC-bus capacitor discharge strategy using internal winding and external bleeder for surface-mounted PMSM-based EV powertrains in emergency," *IEEE Trans. Ind. Electron.*, vol. 68, DOI 10.1109/TIE.2020.2975479, no. 3, pp. 1905-1915, Mar, 2021.

[7] J. Lu, X. Zhang, Y. Hu, J. Liu, C. Gan, and Z. Wang, "Independent phase current reconstruction strategy for IPMSM sensorless control without using null switching states," *IEEE Trans. Ind. Electron.*, vol. 65, DOI 10.1109/TIE.2017.2767542, no. 6, pp. 4492–4502, Jun. 2018.

[8] Y. H. Hu, S. S. Zhu, C. Liu, and K. Wang, "Electromagnetic performance analysis of interior PM machines for electric vehicle applications," *IEEE Trans. Energy Convers*., vol. 33, DOI 10.1109/TEC.2017.2728689, no. 1, pp. 199-208, Mar. 2018.

[9] X. D. Liu, H. Chen, J. Zhao, and A. Belahcen, "Research on the performances and parameters of interior PMSM used for electric vehicles," *IEEE Trans. Ind. Electron.*, vol. 63, DOI 10.1109/TIE.2016.2524415, no. 6, pp. 3533–3545, Jun. 2016.

[10] C. G. Ma, Q. Li, L. W. Deng, *et al.*, "A novel sound quality evaluation method of the diagnosis of abnormal noise in interior permanent-magnet synchronous motors for electric vehicles," *IEEE Trans. Ind. Electron.*, vol. 64, DOI 10.1109/TIE.2017.2652718, no. 5, pp. 3883–3891, May. 2017.

[11] M. Kimiabeigi, J. D. Widmer, R. Long, *et al.*, "High-performance low-cost electric motor for electric vehicles using ferrite magnets," *IEEE Trans. Ind. Electron.*, vol. 63, DOI 10.1109/TIE.2015.2472517, no. 1, pp. 113–122, Jan. 2016.

[12] S. Khan, S. S. H. Bukhari, and J. S. Ro, "Design and analysis of a 4-kW two-stack coreless axial flux permanent magnet synchronous machine for low-speed applications," *IEEE Access*, vol. 7, DOI 10.1109/ACCESS.2019.2957046, pp. 173848-173854, Dec. 2019.

[13] F. G. Capponi, G. D. Donato, and F. Caricchi, "Recent advances in axial-flux permanent-magnet machine technology," *IEEE Trans. Ind. Appl.*, vol. 48, DOI 10.1109/TIA.2012.2226854, no. 6, pp. 2190-2205, Nov./Dec. 2012.

[14] J. J. Chang, Y. N. Fan, J. L. Wu, and B. Zhu, "A yokeless and segmented armature axial flux machine with novel cooling system for in-wheel traction applications," *IEEE Trans. Ind. Electron*., vol. 68, DOI 10.1109/TIE.2020.2982093, no. 5, pp. 4131-4140, May. 2021.

[15] W. M. Tong, S. Wang, S. H. Dai, S. N. Wu, and R. Y. Tang, "A quasi-three-dimensional magnetic equivalent circuit model of a double-sided axial flux permanent magnet machine considering local saturation," *IEEE Trans. Energy Convers*., vol. 33, DOI 10.1109/TEC.2018.2853265, no. 4, pp. 2163-2173, Dec. 2018.

[16] J. H. Kim, W. Y. Choi, and B. Sarlioglu, "Closed-form solution for axial flux permanent-magnet machines with a traction application study," *IEEE Trans. Ind. Appl*., vol. 52, DOI 10.1109/TIA.2015.2496877, no. 2, pp. 1775-1784, Mar./Apr. 2016.

[17] J. H. Choi, J. H. Kim, D. H. Kim, and Y. S. Baek, "Design and parametric analysis of axial flux PM motors with minimized cogging torque," *IEEE Trans. Magn*, vol. 45, DOI 10.1109/TMAG.2009.2018696, no. 6, pp. 2855-2858, Jun. 2009.

[18] S. M. Mirimani, A. Vahedi, F. Marignetti, "Effect of inclined static eccentricity fault in single stator-single rotor axial flux permanent magnet machines," *IEEE Trans. Magn*., vol. 48, DOI 10.1109/TMAG.2011.2161876, no. 1, pp. 143-149, Jan. 2012.

[19] W. L. Zhao, T. A. Lipo, and B. I. Kwon, "Comparative study on novel dual stator radial flux and axial flux permanent magnet motors with ferrite magnets for traction application," *IEEE Trans. Magn*., vol. 50, DOI 10.1109/TMAG.2014.2329506, no. 11, Art. ID. 8104404, Nov. 2014.

[20] R. Wilson, R. Gandhi, A. Kumer, and R. Roy, "Performance analysis of twin-rotor axial flux permanent magnet synchronous motor for in-wheel electric vehicle applications with sensorless optimized vector control strategy," in *IEEE International Conference on Power Electronics, Drives and Energy System (PEDES)*, DOI 10.1109/PEDES49360.2020.9379464, Jaipur, India, Dec. 2020.

[21] M. Aydin, and M. Gulec, "A new coreless axial flux interior permanent magnet synchronous motor with sinusoidal rotor segments," *IEEE Trans. Magn*., vol. 52, DOI 10.1109/TMAG.2016.2522950, no. 7, Art. ID. 8105204, Jul. 2016.

[22] G. D. Donato, F. G. Capponi, and F. Caricchi, "Fractional-slot concentrated-winding axial-flux permanent-magnet machine with core-wound coils," *IEEE Trans. Ind. Appl*., vol. 48, DOI 10.1109/TIA.2011.2182024, no. 2, pp. 630-641, Mar./Apr. 2012.

[23] C. X. Gao, M. Z. Gao, J. K. Si, H. C. Feng, and W. P. Cao, "A novel direct-drive permanent magnet synchronous motor with toroidal windings," *Energies*, vol. 12, DOI 10.3390/en12030432, no. 3, Art. ID. 432, Feb. 2019.

[24] Y. Q. Wei, J. K. Si, Z. P. Cheng, *et al.*, "Design and characteristic analysis of a six-phase direct-drive permanent magnet synchronous motor with 60deg phase-belt toroidal winding configuration for electric vehicle," *IET*

Elec. Power Appl., vol. 14, DOI 10.1049/iet-epa.2020.0083, no. 13, pp. 2659-2666, Dec. 2020.

[25] F. L. Jin, J. K. Si, Z. P. Cheng, *et al.*, "Analysis of a six-phase direct-drive permanent magnet synchronous motor with novel toroidal windings," in *IEEE Vehicle Power and Propulsion Conference (VPPC)*, DOI 10.1109/VPPC46532.2019.8952311, Hanoi, Vietnam, 2019.

[26] J. K. Si, Z. G. Yan, R. Nie, S. Xu, and L. H. Dong, "Optimal design of a tubular permanent magnet linear generator with 120° phase belt toroidal windings for detent force reduction," *Transactions of China Electrotechnical Society*, vol. 36, DOI 10.19595/j.cnki.1000-6753.tces.201077, no. 6, pp. 1138-1148, Mar. 2021.

[27] H. Y. Lee, E. C. Lee, S. O. Kwon, and J. P. Hong, "A study on brushless PM slotless motor with toroidal winding," in *IEEE International Electric Machine and Drives Conference* (IEMDC), DOI 10.1109/IEMDC.2017.8002376, Miami, FL, USA, 2017.

[28] M. C. Sun, R. Y. Tang, X. Y. Han, W. M. Tong, "Analysis of open circuit back electromotive force in slotless toroidal type winding axial flux permanent magnet machine," *Electric Machine & Control Application*, vol. 44, DOI 10.3969/j.issn.1673-6540.2017.09.001, no. 9, pp. 1-8, 2017.

[29] S. D. Huang, S. Y. Cheng, D. R. Luo, *et al*., "Design and characteristic analysis of an axial-flux permanent magnet synchronous motor with contra-rotating rotors," *Transactions of China Electrotechnical Society*, vol. 32, DOI 10.19595/j.cnki.1000-6753.tces.161166, no. 23, pp. 72-80, Dec. 2017.

[30] S. R. Huang, J. Luo, F. Leonardi, and T. A. Lipo, "A comparison of power density for axial flux machines based on general purpose sizing equations," *IEEE Trans. Energy Convers*., vol. 14, DOI 10.1109/60.766982, no. 2, pp. 185-192, Jun. 1999.

Jikai Si (M'20) received the B.S. degree in electrical engineering and automation from the Jiaozuo Institute of Technology, Jiaozuo, China, in 1998; the M.S. degree in electrical engineering from Henan Polytechnic University, Jiaozuo, China, in 2005; and the Ph.D. degree in 2008 from the School of Information and Electrical Engineering, China University of Mining and Technology, Xuzhou, China, in 2008.

He is currently a distinguished professor at Zhengzhou University. His main research interests include the theory, application, and control of special motor. He has authored and co-authored over 160 technical papers in these areas. Prof. Si is a Member of the Green Motor System Professional Committee, China.

Tianxiang Zhang was born in Nanyang, Henan, China in 1997. He received the B.S. degree in electrical engineering from Zhengzhou University of Light Industry, Zhengzhou, in 2019. He is currently working torward the M.S. degree in School of Electrical Engineering of Zhengzhou University, Zhengzhou, Henan.

His research interests include design, analysis and control of axial-flux permanent magnet motors.

Yihua Hu (M'13-SM'15) received the B.S. degree in electrical motor drives, in 2003, and the Ph.D. degree in power electronics and drives, in 2011, both from China University of Mining and Technology, Jiangsu, China. Between 2011 and 2013, he was a Postdoctoral Fellow with the College of Electrical Engineering, Zhejiang University, Zhejiang, China.

He is currently a distinguished professor at University of York. His research interests include PV generation system, power electronics converters and control, and electrical motor drives.

Chun Gan (M'14) received the Ph.D. degree in electrical engineering and motor drives from Zhejiang University, Hangzhou, China, in 2016.

He is currently a Professor with the School of Electrical and Electronic Engineering, Huazhong University of Science and Technology, Wuhan, China. His research interests include electrical motor drives, electrical motor design, electric vehicles, hybrid vehicles, and high-efficiency power converters His current research interests include the theory, application, and control of special motor and power electronics.

Yingsheng Li currently works in Zhengzhou Runhua Intelligent Equipment Co., Ltd, and is the legal representative of Zhengzhou Runhua Intelligent Equipment Co., Ltd. His research interests include the application, control of motor, and power electronics converters and control, and electrical motor drives.